J Appl Electrochem (2009) 39:887–897
DOI 10.1007/s10800-008-9738-5

ORIGINAL PAPER

# Electrochemical, SEM and XPS investigations on phosphoric acid treated surgical grade type 316L SS for biomedical applications

**K. Prabakaran · S. Rajeswari**

Received: 2 February 2008 / Accepted: 21 November 2008 / Published online: 16 December 2008


**Abstract** A simple surface pre-treatment method was attempted to establish a stable passive layer on the surface of surgical grade stainless steel (SS) of type 316L for biomedical applications. Surgical grade type 316L SS specimens were subjected to $H_3PO_4$ treatment for 1 h by completely immersing them in the acid solutions to develop a passive barrier film. The effect of various concentrations of phosphoric acid on the localized corrosion resistance behavior of type 316L SS was investigated through electrochemical techniques using cyclic polarization studies and electrochemical impedance spectroscopy (EIS). X-ray photoelectron spectroscopy (XPS) was used to evaluate the nature and composition of the passive films. The surface morphology and relative elemental composition of the untreated and acid treated surfaces subjected to anodic polarization was studied by scanning electron microscopy (SEM) and energy dispersive X-ray analysis (EDAX) techniques, respectively. Compared with untreated (pristine) 316L SS, the 40% acid treated surface formed a stable passive layer that had superior corrosion resistance.

**Keywords** Type 316L SS · Phosphoric acid treatment · Polarization · Impedance · XPS

## 1 Introduction

Surgical grade stainless steel (SS) of type 316L SS is an important implant material employed both in orthopaedics and dentistry for bone screw/plate, intra-medullary rod, fixation wire, hip joint, and knee joint due its high corrosion resistance, low cost and ease of fabrication. The high corrosion resistance of this material is primarily due to the passive barrier film formed on its surface, for this reason passivation is a question of considerable technical and economical importance. Some authors have suggested that the improvement is the result of chromium enrichment in the passive film [1, 2], or is related to the chromium content and to other elements which may constitute the passive film [1]. However, clinical experiences have shown that the passive layers are susceptible to localized corrosion in physiological environments causing release of metal ions into the tissues and loosening of the implant. Several incidences of failures [3, 4] of such devices have demanded the application of surface modification of alloys.

Since the corrosion resistance of stainless steels depends among other parameters on the surface state, different kinds of surface pre-treatments have been developed to increase the corrosion resistance. Such treatments include pickling, bright annealing, polishing, passivation in alkali and acid media etc. The primary aim of the surface treatment is to enhance the protective passive film by changing its composition, structure and thickness, and or by reducing weak points such as non-metallic inclusions [5].

Several authors have studied the effect of alkali [6–8] and acid treatment on metals. Noh et al. [9] have reported that both the enrichment of chromium oxide on the surface and removal of MnS from the surface of 316L SS take place during nitric acid passivation. Similarly, impedance and XPS studies of surface modification of 316LVM stainless steel after passivation by Wallinder et al. [5] suggested that the passivation treatment significantly increases the corrosion resistance due to the high Cr content in the passive film. Examination of $H_2SO_4$ passivation of stainless steels by Peled et al. [10] also ensures a passive film which resists pit initiation.

K. Prabakaran (✉) · S. Rajeswari
Department of Analytical Chemistry, University of Madras, Guindy Campus, Chennai 600 025, Tamilnadu, India
e-mail: chitrapraba07@gmail.com

Despite the development of many efficient techniques as a research tool for the analysis of passive films, the role of alloying elements other than chromium remains a matter of debate. Electrochemical behavior of the implant materials in physiological media is necessary to assess the corrosion resistance behavior of passive films formed. However, data on the electrochemical behavior of phosphoric acid ($H_3PO_4$) treatment on surgical grade type 316L SS is still scarce. Hence the present work aimed to investigate the effect of $H_3PO_4$ acid treatment on surgical grade type 316L SS in Ringer's solution. Cyclic polarization and electrochemical impedance spectroscopy (EIS) were used to carry out the corrosion studies. The study then evaluated the nature and composition of both untreated and $H_3PO_4$-treated 316L SS by X-ray photoelectron spectroscopy (XPS). The surface morphology and the relative concentrations of the elements present on the surfaces of the pristine and $H_3PO_4$-treated 316L SS were examined using scanning electron microscopy (SEM) and energy dispersive X-ray analysis (EDAX) techniques, respectively.

## 2 Experimental

### 2.1 Sample preparation and surface treatment

Type 316L SS was used as the metal substrate; the elemental composition is given in Table 1. Prior to experiments, the 316L SS specimens ($1 \times 1 \times 0.3$ cm$^2$ in size) were mechanically abraded in sequence with ≠320, ≠400, ≠600, ≠800, SiC paper followed by 5 μm diamond paste to mirror finish. The specimens were washed thoroughly with running distilled water and ultrasonically degreased with acetone. The polished specimens were examined under an optical microscope for the presence of scratches on the surface. Acid treatment was performed by soaking the metal specimens in analar grade $H_3PO_4$ (sp. gr. 1.75) acid solution for 1 h in different volume concentrations varying from 10% to 50% and 80% at ambient temperature. After the acid treatment the specimens were gently washed with distilled and dried at 100 °C for 30 min in an air atmosphere.

### 2.2 Electrochemical corrosion studies

Open circuit potential (OCP)-time measurements, cyclic polarization and EIS experiments were carried out for the evaluation of the untreated (pristine) and $H_3PO_4$-treated 316L SS surfaces. The localized corrosion behavior of the samples was studied in Ringer's solution (NaCl—8.6 g/L, $CaCl_2 \cdot 2H_2O$—0.66 g/L and KCl—0.6 g/L) which simulates body fluid conditions. A 500 ml capacity electrochemical cell fitted with a saturated calomel electrode (SCE) as reference electrode, platinum foil as auxillary electrode and the specimen (1 cm$^2$ exposed surface) as working electrode were used for all electrochemical measurements. The pH of the electrolyte was adjusted to 7.4 and it was maintained at 37 °C. OCP-time measurements and cyclic polarization studies were carried out using a VIBRANT potentiosat/galvanostat (model VSM/CS/30) electrochemical interface controlled by commercial software. The polarization study was carried out once the samples reached the steady state potential by increasing the potential from rest potential towards noble direction at a scan rate of 1 mV s$^{-1}$ until the break down potential ($E_b$) was attained where the alloy entered the passive/transpassive region. The sweep direction was then reversed till the scan entered the passive region. The potential at which the reverse scans meet the passive region is termed the pit repassivation potential or pit protection potential ($E_p$). The potential at which there was a monotonic increase in the current density is termed the break down potential ($E_b$). EIS analysis was performed at room temperature in Ringer's solution using a CHI 660B electrochemical workstation (CH Instruments, USA) controlled by an IBM personal computer.

### 2.3 SEM analysis

Scanning electron microscopy (JEOL, model 6400 microscope, Japan) equipped with a Tracer series II X-ray and image analysis system for energy dispersive X-ray (EDAX) was used to examine the surface morphology and changes in elemental composition, respectively, of the pristine and $H_3PO_4$-treated (various concentrations) 316L SS specimens.

### 2.4 XPS analysis

The specimen treated with 40% phosphoric acid for 1 h was rinsed with double distilled water and then with acetone. After drying at 100 °C for 30 min, the sample was kept in a desiccator until it was transferred into the vacuum controlled chamber of the (KRATOS ESCA model Axis

**Table 1** Elemental composition of type 316L SS (wt.%)

| Element | Cr | Ni | Mo | Mn | P | C | S | Si | Fe |
|---|---|---|---|---|---|---|---|---|---|
| Composition of 316L SS | 18.34 | 12.59 | 2.26 | 1.85 | 0.040 | 0.02 | 0.01 | 0.15 | Balance |
| From ASTM | 16–18 | 12–14 | 2.00 | 2.00 | 0.075 | 0.02 | 0.03 | 1.00 | Balance |

165) XPS unit for analysis. XPS analysis was performed using AlKα X-ray radiation source with a mean energy of 1,486.6 eV at a vacuum of $10^{-7}$–$10^{-9}$ Torr. The output of the photoelectron spectroscopic analysis was obtained as binding energy versus relative intensity count spectrum through a data acquisition system, which was directly interfaced to the XPS unit. The survey spectra were first recorded to identify all the elements present in the surface of the pristine and $H_3PO_4$-treated metal surface. Later, high-resolution spectra were taken for O 1*s*, Fe 2*p*, Cr 2*p*, Ni 2*p*, P 2*p*, and Mo 3*d* electrons. The binding energies of the alloying elements were calculated from the spectra obtained for the respective elements and then the values were corrected for charge shifting with respect to the C 1*s* line from the adventitious carbon at 284.6 eV. Deconvolution of the peaks was attempted by noting the binding energy values at locations where there was a change in the slope of the curve. The binding energy, B.E, scale of the instrument was calibrated on Au and Cu: B.E (Au $4f_{7/2}$) = 84.0 eV; B.E (Cu $2p_{3/2}$) = 932.7 eV.

## 3 Results and discussion

### 3.1 OCP—time measurements

The OCP curves of the samples in Ringer's solution measured as a function of time in comparison with pristine 316L SS are shown in Fig. 1. The OCP-time measurements were recorded as soon as the samples were immersed in the electrolyte. The initial potentials of the samples were noted and monitored as function of time until the samples reached a steady state or stable potential. The steady state potential is the potential at which the metal dissolution (anodic) and electronation (cathodic) reaction rates are equal [11]. Over time, the OCP of the pristine 316L SS sample was found to show a shift in an active direction with a small negative shift at the beginning before it attained a steady state value. In contrast, for the $H_3PO_4$-treated samples, the OCP value shifted in the noble direction (positive potential), which indicates that the treated samples have better corrosion resistance. It is evident from the figure that the OCP for the $H_3PO_4$-treated 316L SS attained a steady state value after a lapse of 8–10 min and 40% $H_3PO_4$-treated 316L SS shows a maximum shift compared to others. A continuous decrease in OCP value was observed for the specimens treated with higher concentration of $H_3PO_4$ (50 and 80%) indicating that the OCP value decreases (marginally) with increase in concentration beyond 40%. Thus, the OCP curves for 40% $H_3PO_4$-treated 316L SS showing more positive shift indicates that the surface possess greater ability to resist the localized attack compared to all other treatments.

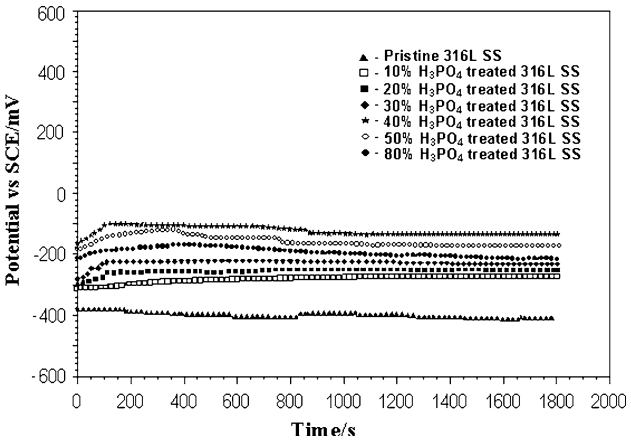


**Fig. 1** OCP-time measurement curves in Ringer's solution for 316L SS treated with various concentrations of $H_3PO_4$

### 3.2 Cyclic polarization studies

The cyclic polarization curves for pristine 316L SS and $H_3PO_4$-treated 316L SS are shown in Fig. 2 and the corresponding electrochemical parameters are illustrated in Table 2. There is a remarkable shift in the $E_b$ value for the acid treated 316L SS compared to that of pristine 316L SS ($E_b$ = +320 mV). Especially, the 40% $H_3PO_4$-treated surface recorded a maximum $E_b$ value of +723 mV (Table 2). Immersion above 40% $H_3PO_4$ causes a decrease in $E_b$ (691 and 669 mV for 50 and 80%, respectively). Hence 40% $H_3PO_4$-treated 316L SS was chosen as the optimum treatment condition for HAP coating. The surfaces treated with higher concentration of acid effects the rapid and extensive dissolution of the passive layer and

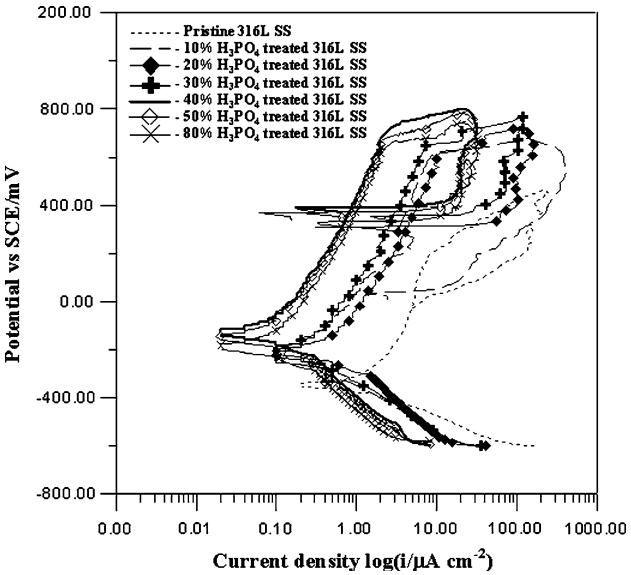


**Fig. 2** Cyclic polarization curves for various concentrations of $H_3PO_4$-treated 316L SS in Ringer's solution

**Table 2** Polarization (cyclic) parameters of 316L SS treated with various concentrations of $H_3PO_4$

| S. No. | Materials | Polarization parameters at OCP | |
|---|---|---|---|
| | | $E_b$/mV | $E_p$/mV |
| 1. | Pristine 316L SS | +320 | −22 |
| 2. | 10% $H_3PO_4$-treated 316L SS | +619 | +32 |
| 3. | 20% $H_3PO_4$-treated 316L SS | +631 | +320 |
| 4. | 30% $H_3PO_4$-treated 316L SS | +652 | +355 |
| 5. | 40% $H_3PO_4$-treated 316L SS | +723 | +393 |
| 6. | 50% $H_3PO_4$-treated 316L SS | +691 | +380 |
| 7. | 80% $H_3PO_4$-treated 316L SS | +669 | +344 |

hence the metal dissolution occurred. A significant weight loss of metal to about 0.004 g and 0.0053 g for 50 and 80% $H_3PO_4$ treatment, respectively, confirms dissolution. Earlier studies have also reported that the metal starts to corrode after a particular concentration [12].

It is generally accepted that the passive layers on stainless steels are actually hydrated oxides [13]. Their stability depends on the alloy composition and on the surrounding environment (purity of water, presence of $Cl^-$ ions and other anions, pH, temperature, etc.). The passive layers contain various oxidative species, but among them, with regard to alloy stability, the chromium oxide layer species play a significant role [14]. It is well known that the surface treatments enhance the protective passive film and hence the corrosion resistance. The selective dissolution of the metal leads to a change in metallurgical composition of the passive film and hence it will be always different from those of substrates. Several authors have suggested that improvement in the corrosion resistance of stainless steels is the result of chromium enrichment in the passive film during acid treatments [2, 15]. Guenbour et al. [16, 17] have investigated the composition of passive film formed on $H_3PO_4$-treated stainless steels. They have reported that the passive film contains Fe, Cr, Ni, P, H, and O under various oxidation states such as $Fe^{2+}$, $Fe^{3+}$, $Cr^{3+}$, $Ni^{2+}$, $P^{5+}$, $OH^-$, and $O^{2-}$ among others. The high concentration of oxygen in surface of stainless steels is generally the result of the formation of metallic oxides [18]. Here, this result can also be explained by the adsorption of phosphate ions on the surface. Lakatos-Varsányi et al. [19] have also reported the formation of $CrPO_4 \cdot 2H_2O$ and Fe–Cr hydroxide during exposure of stainless steels to phosphate containing solution. Our results are in good agreement with their results.

The polarization study also shows that there is a remarkable increase in repassivation potential ($E_p$) for $H_3PO_4$-treated 316L SS compared to pristine 316L SS (Table 2). Dissolution of the covering compound and the mixing of the pit and bulk electrolytes govern repassivation of the pit. Caroll et al. [20] have examined nucleation, growth and the subsequent repassivation of metastable pits on different qualities of stainless steel. They concluded that it is the pit geometry and the composition of the bulk solution, which determine the repassivation process. In the present study, the repassivation obtained with scanning the potential in the cathodic direction is found to be lower when 316L SS is treated with $H_3PO_4$ compared to untreated 316L SS. It could be argued that the high repassivation of the pits in the $H_3PO_4$-treated 316L SS is due to the formation of a phosphate layer on the surface of the pit walls as Cr-phosphates [19].

### 3.3 SEM and EDAX analysis

SEM micrographs for pristine and $H_3PO_4$ (various concentrations) treated 316L SS subjected to anodic polarization are shown in Fig. 3. The morphology of the pits of the corroded samples was evaluated in terms of pit dimensions and depth. It is clear from the micrographs that the untreated surface exhibited individually larger and deeper pits (Fig. 3a) indicating higher susceptibility of the material to pitting attack. However, 40% $H_3PO_4$-treated surface (Fig. 3e) resulted in a very low number of pits compared to pristine and all other treatments (Fig. 3b–f) due to enrichment of the passive layer by alloying elements.

The SEM study clearly shows that material with greater corrosion resistance exhibit a lower depth of pitting attack, whereas materials with lesser corrosion resistance reveal a greater depth of pitting attack. This may be attributed to a low pH within the pits of pristine 316L SS as reported by Ives et al. [21]. According to their findings, when the passive film breaks down at certain weak kink sites, the metal starts to dissolve at a very high rate. Among the alloy constituents, iron dissolves first. Hydrolysis of the metal ions then increases the acidity of the local solution in the vicinity of the pit site. For example, the reactions occur:

$$Fe^{2+} + H_2O \rightarrow FeOH^+ + H^+ \quad (1)$$

$$Fe^{2+} + 2H_2O \rightarrow Fe(OH)_2 + 2H^+ \quad (2)$$

$$3Fe^{2+} + 2H_2O \rightarrow Fe_3O_4 + 4H^+ \quad (3)$$

This acidification accelerates the anodic dissolution at the pit site. The faster dissolution in turn helps to further increase the acidity. Thus, the autocatalytic effect expedites pit formation and development. On the other hand, the resistance to pitting attack by the acid treated specimens may be attributed to enrichment by one of the alloying elements, nickel at their surfaces. Rajendran et al. [22] have reported that hydrolysis of nickel leads to the formation of nickel oxide film according to the reaction:

$$Ni + H_2O \rightarrow NiO + 2H^+ + 2e^- \quad (4)$$

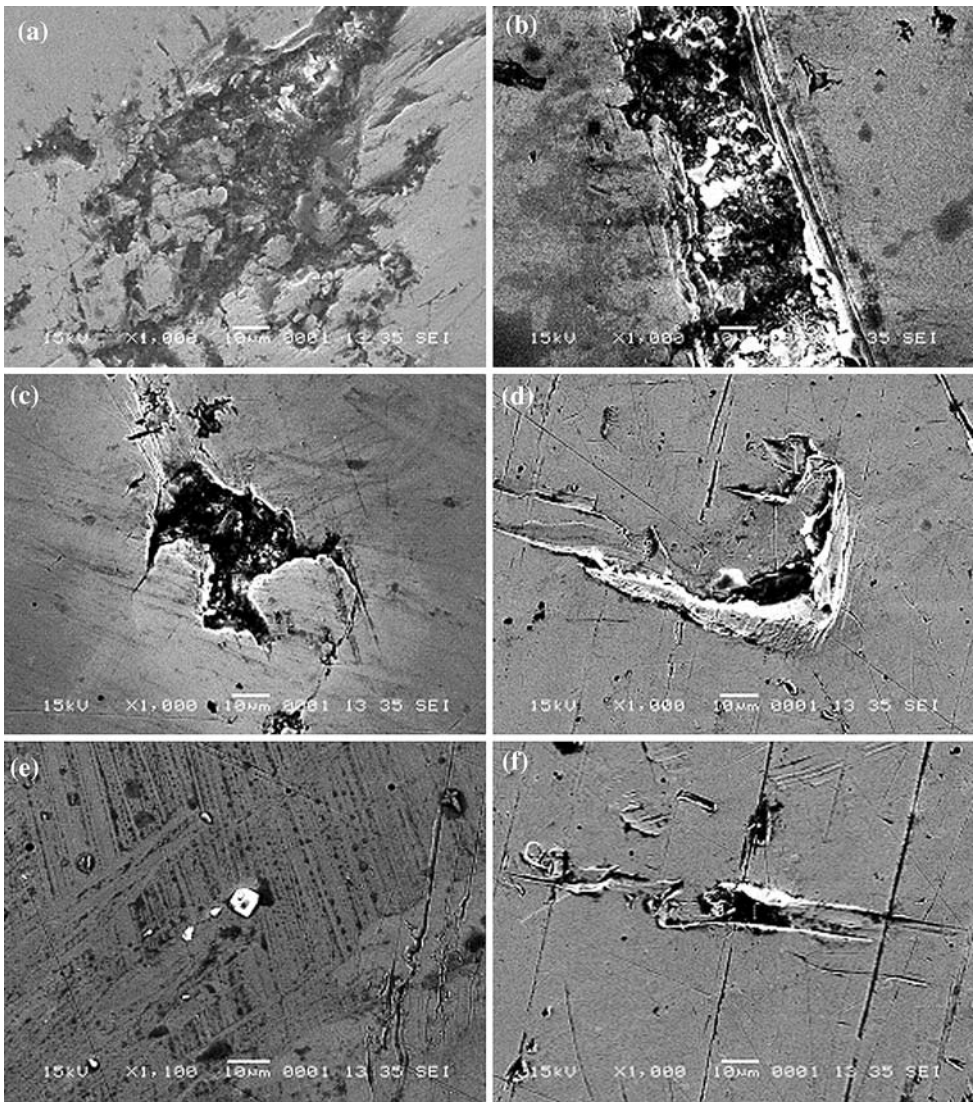


**Fig. 3** SEM micrographs of (**a**) pristine 316L SS and (**b**) 10% (**c**) 20% (**d**) 30% (**e**) 40%, and (**e**) 50% $H_3PO_4$-treated 316L SS surfaces after polarization in Ringer's solution

where there is a direct electrochemical reaction between the working electrode and water in the solution. The hydrolysis of $Ni^{2+}$ yields essentially a neutral pH, so that the dissolved nickel ions are likely to contribute to acidification of the solution within the pit. As a result, the aggressiveness of the environment within the pit is reduced.

The results of the EDAX analysis carried out in the present investigation for examining the changes in the elemental composition on the surface due to acid treatment are illustrated in Table 3. It is clear that the relative concentration (wt.%) of the elements Cr, Mo, Ni, and O is higher for 40% acid treated 316L SS compared to all other samples and favors the stability of the passive film.

**Table 3** Relative concentrations (wt.%) of elements due to $H_3PO_4$ treatment conditions on surgical grade type 316L SS obtained from EDAX analysis

| S. No. | Materials | Fe | Cr | Ni | Mo | O |
|---|---|---|---|---|---|---|
| 1. | Pristine 316L SS | 66.64 | 20.34 | 8.13 | – | 4.89 |
| 2. | 10% $H_3PO_4$-treated 316L SS | 64.47 | 20.73 | 9.26 | 0.56 | 4.98 |
| 3. | 20% $H_3PO_4$-treated 316L SS | 63.88 | 20.86 | 9.43 | 0.72 | 5.11 |
| 4. | 30% $H_3PO_4$-treated 316L SS | 63.45 | 21.05 | 9.51 | 0.79 | 5.20 |
| 5. | 40% $H_3PO_4$-treated 316L SS | 61.67 | 21.86 | 9.79 | 0.95 | 5.73 |
| 6. | 50% $H_3PO_4$-treated 316L SS | 62.59 | 21.52 | 9.62 | 0.83 | 5.44 |

Average of data obtained from several different points on the surface

## 3.4 EIS analysis

Figure 4a shows typical Nyquist plots obtained for untreated and $H_3PO_4$ (various concentrations) treated 316L SS in Ringer's solution. The impedance spectra shown in Fig. 4 for surface treated 316L SS indicate high corrosion resistance towards pristine 316L SS and, in comparison with other surface treatments, 40% $H_3PO_4$-treated 316L SS exhibits better corrosion resistance. Table 4 illustrates the

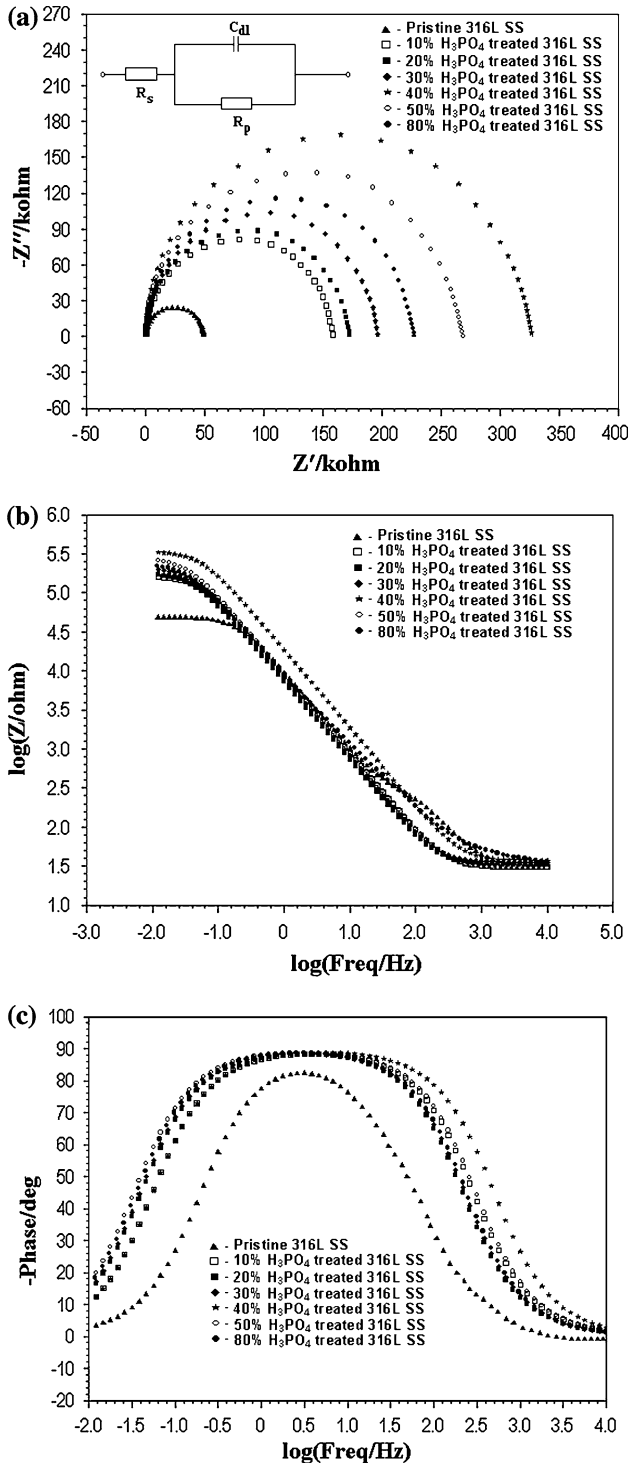


**Fig. 4** Impedance spectra in Ringer's solution for various concentrations of $H_3PO_4$-treated 316L SS (**a**) Nyquist (**b**) Bode |Z| and (**c**) Bode phase plots

impedance parameters obtained for untreated and surface treated 316L SS by fitting the data to Randles circuit (Fig. 5a inset). Consistent values of solution (electrolyte) resistance ($R_s$) are noted for all samples in Ringer's solution. The high $R_p$ value is an indication of the working electrode strongly resisting a change from its equilibrium state and corresponds to a low rate of ionic release and oxide growth. From Table 4 it can also be seen that, in general, all the surface treatments in phosphoric acid solution result in high values of $R_p$ ranging from 0.1623 to 0.3382 Mohm $cm^2$ compared to pristine 316L SS (0.0488 Mohm $cm^2$), which implies excellent corrosion resistance of 316L SS after surface modification. The high corrosion resistance attributed to the protective passive layer on the metal surface (discussed in polarization experiment) manifested in the high values of polarisation resistance ($R_p$) obtained for the treated 316L SS.

Similarly, the total impedance, |Z| for 40% $H_3PO_4$-treated surface has a value of $4.887 \times 10^4$, which is very high compared with that of the untreated surface ($|Z| = 1.760 \times 10^4$). Table 4 shows the values of the double layer capacitance ($C_{dl}$) obtained by curve fitting the EIS data. The film capacitance corresponds to the stability of the passive oxide layer formed on 316L SS. For acid treated 316L SS, the values of $C_{dl}$ in the range 8.57–27.97 μF $cm^{-2}$ were determined. Ionipa et al. [23] evaluated titanium alloys and reported that the lower values of $C_{dl}$ correspond to a slow growth of the oxide film indicating long-term stability of the passive layer. Hence, it can be argued that the possible reason for high |Z| and low $C_{dl}$ may be the enrichment of passive film with Cr, Ni, Mo, P, and O (confirmed by XPS) on the surface treated 316L SS, which hinders the chloride attack.

In Bode plot spectra, two different graphs, Bode phase and Bode |Z| were plotted against frequency. The Bode |Z| graph (Fig. 4b) of $H_3PO_4$-treated 316L SS show straight lines with the slope approaching −2. The constant increase in resistance may be a consequence of formation of continuous passive film, which maintains a constant electric field within it. A similar trend was observed in the Bode phase graph (Fig. 4c), in which a phase angle close to 90° over a wide range of frequency for $H_3PO_4$-treated 316L SS was obtained towards 80° exhibited by pristine 316L SS over a narrow range of frequency. Thus, the results reveal the near capacitance response of pristine 316L SS. Thus, the impedance results are in good agreement with the results achieved from cyclic polarization studies.

### 3.5 XPS analysis

The electrochemical studies revealed that the improved resistance of the treated surface towards localized corrosion attack is mainly due to the stable passive layer formed on the metal surface. Hence, XPS, also known by the corresponding acronym "ESCA" studies were carried out to furnish information about the nature and composition of the passive film developed on the pristine and $H_3PO_4$-

**Table 4** Impedance parameters in Ringer's solution of 316L SS treated with various concentrations of $H_3PO_4$

| S. No. | Materials | Impedance parameters at OCP | | | |
|---|---|---|---|---|---|
| | | $R_s$/ohm cm$^2$ | $C_{dl}$/μF cm$^{-2}$ | $R_p$/Mohm cm$^2$ | Total $\|Z\| \times 10^4$ |
| 1. | Pristine 316L SS | 22.84 | 45.20 | 0.0488 | 1.760 |
| 2. | 10% $H_3PO_4$-treated 316L SS | 30.76 | 27.97 | 0.1623 | 2.634 |
| 3. | 20% $H_3PO_4$-treated 316L SS | 33.88 | 21.83 | 0.1772 | 2.746 |
| 4. | 30% $H_3PO_4$-treated 316L SS | 35.52 | 19.71 | 0.2070 | 3.000 |
| 5. | 40% $H_3PO_4$-treated 316L SS | 37.17 | 8.570 | 0.3382 | 4.887 |
| 6. | 50% $H_3PO_4$-treated 316L SS | 29.91 | 17.32 | 0.2741 | 3.690 |
| 7. | 80% $H_3PO_4$-treated 316L SS | 34.39 | 19.28 | 0.2312 | 3.211 |

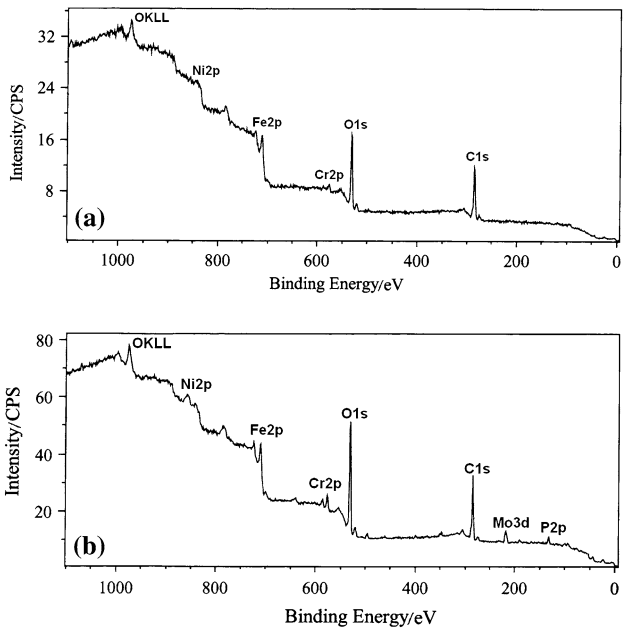


**Fig. 5** XPS survey spectra of (**a**) Pristine 316L SS and (**b**) 40% $H_3PO_4$-treated 316L SS

treated 316L SS. XPS studies showed that the passive film consists mainly of oxides and hydroxides. It also revealed that the major alloying elements contribute to the formation of passive film are Cr, Mo, and Ni. In order to ascertain the factors controlling the chemical composition and the stability of these metallic oxides in the passive film, it is essential to discuss the role played by these elements. Analysis of the passive film by XPS, gives detailed information about composition of the very thin reaction products formed on the surfaces.

Figure 5a shows the XPS spectrum recorded for the pristine 316L SS. The spectrum for the pristine 316L SS shows the peaks corresponding to alloying elements such as Fe, Cr, Ni, C, and O except Mo. However, the spectrum for $H_3PO_4$-treated surface (Fig. 5b) shows the peaks corresponding to all the alloying elements (including Mo) and peak corresponding to 2*p* energy level of P and thus confirmed the enrichment of Mo and P in addition to Cr. The intensities of the count for all elements were also doubled for the treated surface indicating enrichment.

### 3.5.1 Fe 2p spectra

Figure 6a, b represents the XPS spectra for Fe 2*p* of pristine and $H_3PO_4$-treated specimens recorded in the binding energy window 700–740 eV. The pristine 316L SS showed three peaks at 706.8, 711.3, and 723.0 eV. However, $H_3PO_4$-treated 316L SS showed five peaks on deconvolution at 706.8, 709.3, 711.3, 719.2, and 723.0 eV. On the basis of previous reported results, the peaks at 706.8 and 719.2 eV are assigned to $2p_{3/2}$ and $2p_{1/2}$ of metallic iron, respectively [24]. The prominent peaks observed at 711.3 eV for both untreated and treated surface were responsible for $2p_{3/2}$ of $Fe_2O_3$. A couple of peaks at 709.3 and 723.0 eV represent $2p_{3/2}$ and $2p_{1/2}$ of FeOOH, respectively. The oxides of iron that are weakly bonded with water molecules at the top surface layers have resulted in a thin iron oxyhydroxide layer [24]. From the above results, it is inferred that the passive film of untreated and treated specimens consisted of iron in the form of $Fe_2O_3$ and FeOOH.

### 3.5.2 Cr 2p spectra

The high-resolution XPS spectra of the Cr 2*p* energy level recorded in the binding energy values ranging from 560.0 to 610.0 eV for pristine and $H_3PO_4$-treated 316L SS are shown in Fig. 6c, d. Deconvolution of the Cr 2*p* energy level yielded three peaks for pristine and four peaks for treated surface. A pair of prominent peak at binding energy values of 576.3 and 586.0 eV corresponds to the $2p_{3/2}$ and $2p_{1/2}$ of $Cr_2O_3$ [25], respectively. The binding energy values of 577.1 eV for $H_3PO_4$-treated surface may be attributed to $2p_{3/2}$ of chromium hydroxide and chromium phosphate. The metal peak at a binding energy value of 574.4 eV is almost negligible in comparison with the

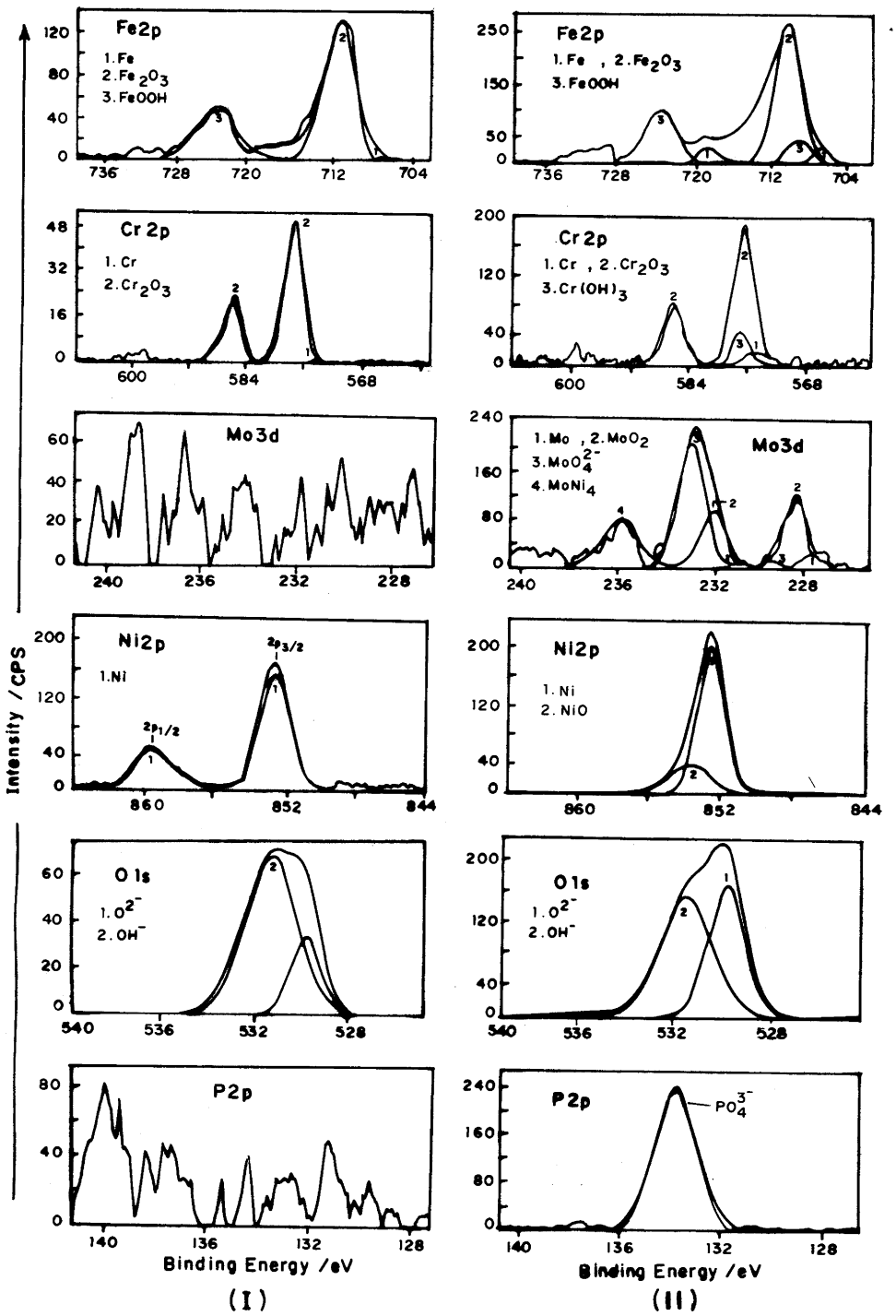


**Fig. 6** XPS spectra of Fe 2*p*, Cr 2*p*, Mo 3*d*, Ni 2*p*, O 1*s* and P 2*p* for (I) Pristine 316L SS and (II) 40% $H_3PO_4$-treated 316L SS

amplitudes of other peaks. The increase in the intensities of the counts corresponding to $Cr_2O_3$ illustrated that the enrichment of oxide layer for treated surface is higher in comparison with pristine 316L SS. It was also observed that in all the above cases, Cr was found as $Cr^{3+}$ in the various forms of oxides and hydroxides at their respective binding energy values, which are in good agreement with earlier reports [26–28].

### *3.5.3 Mo 3d spectra*

Molybdenum, as an alloying element, is known for its role in improving the passivation properties and corrosion resistance of stainless steels [29, 30]. The Mo 3*d* energy levels were analysed in the binding energy region between 226.0 and 241.0 eV to identify the presence of molybdenum and its oxides in the passive films. The molybdenum

3*d* spectra are very complex owing to the fact that various oxidation states exist in the oxide products. Deconvolution of high-resolution spectra of Mo 3*d* electron for pristine and $H_3PO_4$-treated 316L SS are illustrated in Fig. 6e, f. Figure 6e shows that no peaks corresponding to molybdenum at Mo 3*d* region were found which indicates the absence of Mo at the surface of the pristine 316L SS. Whereas the Mo 3*d* spectrum (Fig. 6f) of $H_3PO_4$-treated 316L SS was deconvoluted into three peaks at binding energies of 227.7, 228.7, and 230.0 eV corresponding to the $3d_{5/2}$ energy level of Mo, $MoO_2$ and $MoO_4^{2-}$ species, respectively. Similarly the peaks at 231.0, 232.0, and 233.3 eV represent the $3d_{3/2}$ of Mo, $MoO_2$ and $MoO_4^{2-}$ species, respectively. Apart from the Mo, $Mo^{4+}$, and $Mo^{6+}$ species, a peak was observed at a binding energy of 236.0 eV, which may be attributed to some intermetallic molybdenum species, as proposed earlier by Brewer [31].

### 3.5.4 Ni 2p spectra

The Ni 2*p* spectra were recorded for untreated and treated surface between 836.0 and 864.0 eV and are shown in Fig. 6g, h. The pristine 316L SS showed doublet at 852.8 and 859.9 eV corresponding to the $2p_{3/2}$ and $2p_{1/2}$ of Ni on deconvolution. However, $H_3PO_4$-treated 316L SS exhibits a doublet at 852.8 and 854.4 eV corresponding to metallic Ni and NiO [32–36], respectively. Thus, the XPS analysis of Ni 2*p* clearly indicates that, in the treated surface, nickel is present in the form of metallic Ni and NiO, whereas in the pristine 316L SS, it is present only in the metallic state.

### 3.5.5 O 1s spectra

O 1*s* spectra were recorded for both untreated and treated surface between the binding energy values of 526.0 and 544.0 eV (Fig. 6i, j). The chemical states of oxygen were identified by correlating the observed binding energy values with those of the reported values. The oxygen signal fitted into components representing oxygen bound in oxide, hydroxide, phosphate and water. Two peaks observed for the pristine 316L SS (Fig. 6i) at 530.1 and 531.5 eV correspond to the presence of oxygen in the form of $O^{2-}$ and $OH^-$ species, respectively. The peak at 533.0 eV (Fig. 6j) for the treated surface is reported to be due to the presence of adsorbed water molecules.

### 3.5.6 P 2p spectra

P 2*p* spectra recorded for the untreated and $H_3PO_4$-treated 316L SS in the binding energy window between 127.0 and 141.0 eV are shown in Fig. 6 k, l. The phosphorus 2*p* spectrum of acid treated surface exhibited a singlet at 133.8 eV corresponding to $2p_{3/2}$ of phosphate ($PO_4^{3-}$) species [19]. However, the P 2*p* spectrum of untreated specimen did not show a peak in the P 2*p* region and indicates the absence of $PO_4^{3-}$.

### 3.5.7 Role of alloying elements in the passive film

The analyses of the passive film of pristine and $H_3PO_4$-treated 316L SS surface by XPS revealed that the major alloying elements namely chromium, molybdenum, and nickel were enriched in the passive film as their respective oxides. The exact role played by these elements in aiding the stability of the passive film can be discussed as follows.

From the XPS analysis, it was identified that chromium was the major element present in the passive film along with Mo of the treated surface and its trivalent state can be separated into oxide and hydroxide. Also the intensity of the $Cr_2O_3$ peak was higher in the case of the treated surface in comparison with the untreated surface. Studies of Olefjord and Marcus (34) also suggested that $Cr_2O_3$ is the main passivity compound. Moreover, by comparing the chromium peaks of the $H_3PO_4$-treated surface with that of the pristine material, it was found that $Cr^{3+}$ in the form of $Cr(OH)_3$ was enriched in the passive film of the treated surface. The presence of $Cr_2O_3$ and $Cr(OH)_3$ in the $H_3PO_4$-treated surface indicated that there is an enrichment of chromium at the metal/film interface. The presence of the chromium-rich phase suggests the direct reaction of chromium with water to form $Cr_2O_3$ and perhaps some $CrO_3$, followed by formation of $Cr(OH)_3$ at the oxide-solution interface. These reactions constitute the initial passivation process during polarisation. Earlier results have suggested that the presence of $Cr(OH)_3$ is beneficial in increasing the corrosion resistance in terms of the activity and repassivation of the micropores. The micropores appear to be formed and repassivated repeatedly on the active sites of the underlying alloy where it is difficult to form a stable passive film [26, 36–38]. Increase in chromium content of the $H_3PO_4$-treated surface interferes with the development of micropores into pits due to a rapid repassivation, by forming a passive hydrated $Cr(OH)_3$ and $CrPO_4$. Thus, the presence of higher amounts of chromium in $H_3PO_4$-treated surface could have aided the formation of protective oxide layer, which enhances the localized corrosion resistance of the material. Iron in the form of $Fe_2O_3$ and FeOOH was observed in both the pristine and $H_3PO_4$-treated surface. However, the presence of both the species was higher in the case of the treated surface. FeOOH species stabilise the passive film by preventing the adsorption of halide ions into the film [39, 40]. Since this species is present in large amount in $H_3PO_4$-treated surface compared to pristine 316L SS it is less prone to localized attack.

Nickel is identified mainly in its metallic state for pristine 316L SS. However, nickel was identified in the

form of metallic form and NiO for $H_3PO_4$-treated surface. The oxide film is believed to inhibit nickel dissolution by forming a physical barrier between metal and solution thus preventing bare metal from being in contact with the solution. In recent studies it was also reported that metallic nickel underneath the passive film [41, 42] may contribute to passivation and improved pitting resistance through the formation of intermetallic bonds with Cr and Mo and this reduces anodic dissolution. Halada et al. [43] explained the enrichment of Cr and retention of Ni in the surface layer just beneath the passive film. It was also reported that the formation of a molybdenum–nickel intermetallic phase of the type $MoNi_4$ and its strong Mo–Ni intermetallic bond was the driving force for the enrichment of Mo and Ni during passivation. The Engel–Brewer [31] theory of intermetallic bonding supports the occurrence of such enrichment as a result of the formation of an intermetallic compound of type $MoNi_4$. The intermetallic layer along with the passive film enriched the source of the oxide-forming metallic species directly beneath the passive film and hence may be responsible for the outstanding stability against the localized corrosion attack [33] of the acid treated surface.

Molybdenum enhances the stability of the passive film from the solution side and the presence of Mo in the metal phase near the oxide/metal interface limits the dissolution rate of iron and chromium. It has been reported that molybdenum shows complex oxide chemistry with different states of oxidation. $Mo^{6+}$ is found to be enriched at the microcracks and decreases the size of the active sites, whereas $Mo^{4+}$ shows a more homogenous distribution through out the passive film [44]. Usually, the passive film on a stainless steel surface is heterogeneous and contains high density of microcracks through which current can leak [45]. The microcracks are filled with water and this is responsible for the high current. The study conducted by Lu et al. [46] also ensures that Mo could form $Mo^{6+}$ oxide in the passive film, thereby blocking the penetration of $Cl^-$ ion. The appearance of the $Mo^{4+}$ on the passive film suggests that the first formed barrier layer may be hydrated $MoO_2$ along with $Cr(OH)_3$. It was also reported that formation of $MoO_4^{2-}$ species at the active sites decreases the dissolution of the metal substrate in the presence of $Cl^-$ [47]. Asami et al. [30] and Lu et al. [35, 48] suggested that $MoO_4^{2-}$ anions are responsible for producing a bipolar film consisting of a cation selective outer layer and an intrinsically anion selective inner layer. The bipolarity of the duplex film [49] was considered to be largely responsible for the development of an interfacial barrier layer composed of $Cr(OH)_3$, which resists $Cl^-$ and $OH^-$ ingress. The more abundant $MoO_4^{2-}$ anion may convert the intrinsically anion selective hydrated oxides to cation selective phases. The imposed anodic potential will induce deprotonation of the inner layer resulting in the loss of protons to the solution via the cation selective outer layer.

The electric field enhances the deprotonation of $OH^-$ ions causing the ingress of protons through the cation selective layer and the ingress of remaining $O^{2-}$ anions towards the metal-film interface where reaction with Cr takes place to form $Cr_2O_3$. It has also been reported that the presence of high valence state can compensate the defects created by $Fe^{2+}$ and reduce the pit initiation frequency [33].

Oxygen in the form of $O^{2-}$ and $OH^-$ was observed in the outermost region of the passive film of the metal substrates under study. The mixture of $O^{2-}$ and $OH^-$ ions would contribute to an improvement in the stability of the passive film by occupying the vacant sites and reducing the defect concentration. Hence, higher resistance of the treated surface may be attributed to the presence of these species with higher magnitude. The P-signal corresponds to phosphorous in phosphate formed on the surface of the steel treated with acid. The amount of phosphate on the surface is considerably high. The study conducted by Lakatos-Varsányi et al. [19] suggested that phosphate does not influence the electrochemical parameters such as dissolution current in the active range, the passive current and the pitting potential. However, they further argued that phosphate enhances the repassivation potential by forming chromium phosphate on the surface of the pit walls.

Thus, the enrichment of Cr, Mo, and Ni strongly shifts the anodic polarization curve in the noble direction and reduces local dissolution currents, acidification of the pit embryo and the presence of $CrPO_4$ facilitates repassivation. The combination of these facts explains the outstanding resistance against localized corrosion of the $H_3PO_4$-treated surface compared to that of pristine 316L SS.

## 4 Conclusion

The corrosion resistance behavior of surgical grade of type 316L SS treated with various concentration of $H_3PO_4$ was evaluated using cyclic polarization and EIS measurements. From the results it was found that 40% $H_3PO_4$-treated 316L SS showed better corrosion resistance (high $E_b$, $E_p$, $R_p$, and $|Z|$) than other surface treatment. SEM investigation of the samples after polarization showed that the acid treated surface develops fewer pits with smaller area and depth. EDAX analysis substantiates the presence of Cr, Ni, and Mo (the essential constituents for the enhancement of corrosion resistance) in the passive film. XPS analysis illustrated that the enrichment of Cr, Ni, Mo, and P at the passive film of the treated sample enhances the corrosion resistance. Hence the present work suggests that $H_3PO_4$-treated 316L SS is a better material under implant conditions.

**Acknowledgment** The authors acknowledge the financial support rendered by University Grants Commission (UGC) through University with Potential for Excellence (UWPFE) programme to carry out this work.

## References

1. Salvago G, Fumagalli G (1994) Corros Sci 36:733
2. Asami K, Hashimoto K (1979) Corros Sci 19:1007
3. Sivakumar M, Kamachi Mudali U, Rajeswari S (1994) J Mater Sci Lett 13:142
4. Pholer OEM (1986) ASM Handbook of failure analysis and prevention, 9th edn. ASM International, Metals Park, Ohio
5. Willinder D, Pan J, Leygraf C et al (1999) Corros Sci 41:275–289
6. Deakin J, Dong Z, Lynch B et al (2004) Corros Sci 46:2117
7. Abreu CM, Cristóbal MJ, Losada R et al (2004) Electrochim Acta 49:3049
8. Vuković M (1995) Corros Sci 37:111
9. Noh JS, Laycock NJ, Gao W et al (2000) Corros Sci 42:2069
10. Peled P, Itzhak D (1991) Corros Sci 32:83
11. Bockris JOM, Reddy AKN (1973) Modern electrochemistry—II. Plenum Press, New York
12. Itzhak D, Eghion E (1984) Corros Sci 24:145
13. Okamoto G (1973) Corros Sci 13:471
14. Uhilig HH (1963) Corrosion and corrosion control. Wiley, New York
15. Hultqvist G, Leygraf C (1980) Corrosion 36:126
16. Guenbour A, Faucheu J, Ben Bachir A (1988) Corrosion 44:214
17. Guenbour A, Bui N, Faucheu J et al (1990) Corros Sci 30:189
18. Bellaouchou A, Kabkab B, Guenbour A et al (2001) Prog Org Coat 41:121
19. Lakatos-Varsányi M, Falkenberg F, Olefjord I (1998) Electrochim Acta 43:187
20. Caroll WM, Howley MB, Walsh TM (1989) Proceedings of 9th European congress on corrosion, Utrecht
21. Ives MB, Luo JL, Lu YC (1984) Proceedings of 9th International congress on metallic corrosion, Ottawa
22. Rajendran N, Rajeswari S (1996) J Mater Eng Perform 5:46–50
23. Ionipa D, Santana-Lopez A (2003) Eur Cells Mater 5:12
24. Devaux R, Vouagner D, deBecdelievere AM et al (1994) Corros Sci 36:171
25. Jedrkowski J, Martan J, Masalski J et al (1989) Phys Stat Soli A112:357
26. Brooks AR, Clayton CR, Doss K et al (1986) J Electrochem Soc 133:2459
27. Sugimoto K, Sawada Y (1977) Corros Sci 17:425
28. Childs PE, Laub LW, Wagner JB (1971) Proc Br Ceram Soc 19:21
29. Tullin C, Jungstrom EL (1989) Energy Fuels 3:284
30. Asami K, Hashimoto K, Shimodaira S (1976) J Jpn Inst Met 40:438
31. Brewer L (1968) Science 161:115
32. Halada GP, Clayton CR, Herman H (1995) J Electrochem Soc 142:74
33. Rossi A, Elsener B (1993) Proceedings of 12th International corrosion control, NACE, Houston, Texas
34. Olefjord I, Marcus P (1982) Surf Interface Anal 4:23
35. Lu YC, Clayton CR, Brooks AR (1989) Corros Sci 29:863
36. Dobbelaar JAL, de Wit JHW (1990) J Electrochem Soc 137:2038
37. De Vito E, Marcus P (1992) Surf Interface Anal 19:403
38. Marcus P, Grimal JM (1992) Corros Sci 33:805
39. Grabke HJ (1996) ISIJ Int 36:777
40. Mathieu HJ, Landolt D (1991) Electrochim Acta 36:1623
41. Clayton CR, Castle JL (1977) Corros Sci 17:1
42. Olefjord I, Olfstrom B (1997) Proceedings of 6th European congress on metallic corrosion. Society of chemical industry, London
43. Halada GP, Kim D, Clayton CR (1996) Corrosion 52:36
44. Olsson COA, Hernstrom SE (1994) Corros Sci 36:41
45. Hashimoto K, Asami K, Termoto K (1979) Corros Sci 19:3
46. Lu YC, Ives MB, Clayton CR (1993) Corros Sci 35:89
47. Asami K, Hashimoto K, Masumoto T et al (1976) Corros Sci 16:909
48. Lu YC, Clayton CR (1985) J Electrochem Soc 132:2517
49. Sakashita M, Sato N (1978) In: Frankenthal RP, Kruger J (eds) Passivity of metals. The Electrochemical Society, Pennington, NH